Journal of Nonlinear Modeling and Analysis
Volume 7, Number 3, June 2025, 764–781
https://journal.global-sci.org/jnma
DOI:10.12150/jnma.2025.764

The Dynamics of the Spruce Budworm-Bird System on Time Scale*

Yao Zhang[1] and Yongzhen Pei[1,†]

Abstract We perform a geometric analysis focusing on relaxation oscillations and canard cycles within a singularly perturbed predator-prey system involving budworm and birds. The system undergoes a comprehensive stability analysis, leading to the identification of canard cycles in proximity to the Hopf bifurcation points. The study particularly highlights the transition from smaller Hopf-type cycles to larger relaxation cycles. And the expression of transition threshold $\mu_c(\sqrt{\varepsilon})$ of the spruce budworm-bird system is obtained innovatively. Furthermore, numerical simulations are carried out to validate the theoretical findings.

Keywords Slow-fast timescale, relaxation oscillation, canard cycle, predator-prey system

MSC(2010) 34C26, 35B44, 37G15.

1. Introduction

Relaxation oscillations represent a form of periodic solutions prevalent in slow-fast systems, extensively utilized in modeling chemical and biological processes. These oscillations manifest as sequential cycles characterized by alternating phases of dissipation and abrupt changes. Specifically, within the domain of relaxation oscillations lie the noteworthy phenomena of canard cycles, depicting trajectories within slow-fast systems that persist in proximity to a repelling slow manifold for a duration of $O(1)$ time [1]. Notably, recent years have witnessed a revitalized interest in the study of canard cycles, a resurgence intertwined with both the theoretical underpinnings of dynamical systems and their practical applications.

In the realm of smooth slow-fast systems, the emergence of a Hopf bifurcation occurs when the slow nullcline intersects the fast nullcline transversely, commonly near a fold or local extremum referred to as the critical manifold. This pivotal occurrence transpires particularly when the fast nullcline assumes an 'S'-shaped structure. Subsequently, the evolution of Hopf cycles gradually transforms into relaxation oscillations. This intriguing transition from Hopf cycles to relaxation oscillations takes place within an exponentially minute parameter range, recognized as a canard explosion [2, 3].

†the corresponding author.
Email address:yzhpei@tiangong.edu.cn(Y. Pei)
[1]School of Mathematical Sciences, Tiangong University, Bingshui West Street, Tianjin, China
*The authors were supported by National Natural Science Foundation of China (12371499).

Around the era of 1980, the conception of geometric singular perturbation theory, pioneered by Fenichel [4], explicated the formation and dynamic analysis of canard explosions. This theory adopts a geometric approach in addressing singular perturbation quandaries, prominently involving the crucially significant normally hyperbolic condition. Noteworthy advancements have surfaced in recent years, introducing a prevalent mechanism aimed at scrutinizing instances where the condition of normal hyperbolicity fails. This innovative approach amalgamates blow-up techniques and dynamical systems, originally introduced by Dumortier and Roussarie [5], later harnessed by Krupa and Szmolyan [1].

In recent years, Brons et al. [6,7] conducted an analysis on mixed-mode oscillations arising from canard-type and singular Hopf bifurcations in a model representing a forest pest ecosystem. Izhikevich [8] explored bifurcations in both resting and active states of the burster, introducing a comprehensive theoretical classification method termed 'top-down' fast/slow dynamics bifurcation analysis. This methodology facilitated a meticulous examination and elucidation of diverse bifurcation mechanisms governing discharge rhythm in fast/slow neuron models [9,10].

Since the initial discovery of the correlation between canards and Mixed-Mode Oscillations (MMOs) in neuron models by [11], subsequent research consistently demonstrated and established the potential link between these phenomena [12,13]. A detailed theoretical exposition is provided in the literature [14,15].

It is well-acknowledged that predation can induce oscillations in interacting species, and numerous field and experimental data showcase periodic fluctuations in both predator and prey populations [16]. The existence of limit cycles in predator-prey models has been extensively investigated (see, for instance, [17]). Regarding the presence of relaxation dynamics, pertinent references include [18].

In the realm of biology and ecology, there is notable interest in exploring the dynamics of slow-fast prey-predator systems when the predator's death rate remains exceptionally low. For instance, predator animals like birds may only feed once every two or three hours due to low hunting success. Conversely, prey such as the spruce budworm reproduces rapidly, with a single female capable of producing tens of thousands of offspring in a short period. Their reproductive and mortality rates exhibit considerable variation over the same time frame. Hence, it is judicious to investigate slow-fast predator-prey systems incorporating small parameters.

In this paper, we study relaxation oscillations and canard cycles of the spruce budworm-bird system by combining geometric singular perturbation theory [4] and the Hopf bifurcation Theorem [1]. Specifically, in Section 2, the stability analysis of the system is performed. Then in Section 3 we introduce the slow-fast system. In Section 4 we discussed GSPT and blow-up technique for a detailed mathematical analysis of slow-fast systems. Finally, the conclusion of our work is drew in Section 5.

2. Model and its linear stability analysis

2.1. Predator-prey model

First, the dynamics of the budworm population without the action of predation will be described by the logistic equation

$$\frac{\mathrm{d}\omega}{\mathrm{d}t} = r\omega\left(1 - \frac{\omega}{K}\right),$$

where ω represents the budworm density, r denotes the maximum growth rate of ω,K represents the carrying capacity of the forest. We describe the predation of birds on aphids using the following equation

$$\alpha B \frac{\omega^2}{A^2+\omega^2},$$

which represents a Type-III S-shaped functional response.α signifies the maximum predation rate of an individual bird (on average), B represents the bird density and the parameter A corresponds to the budworm population when the predation rate is at half of its maximum. Therefore, for the dynamic density of budworm under predation by birds, we have the following equation

$$\frac{\mathrm{d}\omega}{\mathrm{d}t} = r\omega\left(1-\frac{\omega}{K}\right) - \alpha B\frac{\omega^2}{A^2+\omega^2}.$$

The above formula has been studied by Ludwig, Jones and Holling [19], under the assumption of a constant bird density B.

In this paper we assume that some birds may leave the system if the budworm population goes down. Let μ denotes the rate at which birds exit the system through migration or death while c quantifies the predation efficiency-defined as the number of new birds generated for each budworm killed. Thus the equation for bird density is given by

$$\frac{\mathrm{d}B}{\mathrm{d}t} = -\mu B + c\alpha\frac{B\omega^2}{A^2+\omega^2}.$$

Combining the above assumptions, the classical budworm-bird model with the Type-III S-shaped functional response is considered [20–22]. Let ω and B be the budworm and bird densities at time t, respectively. The model is given by the following equations:

$$\begin{cases} \dfrac{\mathrm{d}\omega}{\mathrm{d}t} = r\omega\left(1-\dfrac{\omega}{K}\right) - \alpha B\dfrac{\omega^2}{A^2+\omega^2}, \\ \dfrac{\mathrm{d}B}{\mathrm{d}t} = -\mu B + c\alpha\dfrac{B\omega^2}{A^2+\omega^2}. \end{cases} \tag{2.1}$$

We have judiciously selected dimensionless variables and parameters, following the conventions outlined in [23]. The substitutions $\omega = \bar{\omega}A$, $t = \frac{\tau}{c\alpha}$, and $B = cA\bar{B}$ lead to the formulation of the rescaled system

$$\begin{cases} \dfrac{\mathrm{d}\bar{\omega}}{\mathrm{d}\tau} = f\left(\bar{\omega},\bar{B}\right) = \bar{r}\bar{\omega}\left(1-\dfrac{\bar{\omega}}{\bar{K}}\right) - \dfrac{\bar{B}\bar{\omega}^2}{1+\bar{\omega}^2}, \\ \dfrac{\mathrm{d}\bar{B}}{\mathrm{d}\tau} = g\left(\bar{\omega},\bar{B}\right) = -\bar{\mu}\bar{B} + \dfrac{\bar{B}\bar{\omega}^2}{1+\bar{\omega}^2}, \end{cases} \tag{2.2}$$

where $\bar{r} = \frac{r}{c\alpha}$, $\bar{K} = \frac{K}{A}$, $\bar{\mu} = \frac{\mu}{c\alpha}$.

Note that $\bar{\omega}$ signifies the proportion of budworms relative to the variable A, while $\bar{B}$ denotes the ratio between bird density and the product of predation efficiency and A. Additionally, τ represents the time, rescaled by the duration required for birds to consume budworms. Throughout the subsequent sections of this paper, we adopt the simplified notation ω, B, t, r, K, μ, for the rescaled variables $\bar{\omega}$, $\bar{B}$, τ, and parameters $\bar{r}$, $\bar{K}$, $\bar{\mu}$, respectively.

Given the inherent characteristics of species, it is often observed that the prey population exhibits a considerably higher growth rate than its predator. A notable example is illustrated by the interaction between budworms and birds, where budworms manifest a substantially faster reproductive rate than birds. This phenomenon has motivated researchers to introduce a small timescale parameter, denoted as ε with the constraint $0 < \varepsilon \ll 1$, into the foundational model (2.2). The parameter ε is construed as the ratio between the linear death rate of the predator and the linear growth rate of the prey, as discussed by previous studies [24]. The underlying assumption associated with ε posits that a single generation of predators may engage with multiple generations of prey [25]. Consequently, acknowledging the timescale discrepancy, the slow-fast version of the dimensionless model (2.2) is articulated as follows

$$\begin{cases} \dfrac{\mathrm{d}\omega}{\mathrm{d}t} = f(\omega,\ B) = r\omega\left(1 - \dfrac{\omega}{K}\right) - \dfrac{B\omega^2}{1+\omega^2}, \\ \dfrac{\mathrm{d}B}{\mathrm{d}t} = \varepsilon g(\omega,\ B) = \varepsilon\left(-\mu B + \dfrac{B\omega^2}{1+\omega^2}\right). \end{cases} \tag{2.3}$$

Since the prey population grows faster compared to the predator, ω and B are referred to fast and slow variables, respectively, and time t is called fast time.

2.2. Stability analysis

System (2.3) and system (2.2) share identical linear stability results, as the analytical conditions are independent of ε. The equilibria of system (2.2) are as follows:

$$\begin{aligned} E_1 &= (0,0), \\ E_2 &= (K,0), \\ E_3 &= \left(-\frac{\mu}{\sqrt{\mu-\mu^2}}, \frac{r}{\sqrt{\mu-\mu^2}}\left(1 - \frac{\mu}{K\left(\sqrt{\mu-\mu^2}\right)}\right)\right), \\ E_4 &= \left(\frac{\mu}{\sqrt{\mu-\mu^2}}, \frac{r}{\sqrt{\mu-\mu^2}}\left(1 - \frac{\mu}{K\left(\sqrt{\mu-\mu^2}\right)}\right)\right). \end{aligned}$$

It is worth noting that the extinct equilibrium E_1 and the prey-only equilibrium point E_2 always exist. However, since E_3 has negative (or complex) coordinates, it lacks biological significance and is therefore not considered in this context. Regarding E_4, this point holds biological relevance when $0 < \mu < \frac{K^2}{1+K^2}$, as otherwise, negative or non-real populations are managed. The coordinates of E_4 are denoted as (ω^*, B^*), where

$$\begin{aligned} \omega^* &= \frac{\mu}{\sqrt{\mu-\mu^2}}, \\ B^* &= \frac{r}{\sqrt{\mu-\mu^2}}\left(1 - \frac{\mu}{K\left(\sqrt{\mu-\mu^2}\right)}\right). \end{aligned}$$

To assess the stability of the equilibrium point, we linearize system (2.2) by calculating the Jacobian matrix:

$$\begin{pmatrix} r\left(1-\frac{2\omega}{K}\right)-\frac{2B\omega}{(1+\omega^2)^2} & -\frac{\omega^2}{1+\omega^2} \\ \frac{2B\omega}{(1+\omega^2)^2} & \frac{\omega^2}{1+\omega^2}-\mu \end{pmatrix}. \tag{2.4}$$

For a two-dimensional system, stability can be assessed by examining the trace T and determinant Δ of matrix (2.4) evaluated at the equilibrium point. A point is considered stable if $\Delta > 0$ and $T < 0$. In this analysis, we specifically focus on the positive equilibrium E_4.

Theorem 2.1. *For the stability of E_4 (ω^*, B^*), the following results hold.*

(i) E_4 is stable for $\mu < \mu_H$.

(ii) E_4 loses its stability via Hopf bifurcation when $\mu = \mu_H$.

(iii) E_4 is unstable and surrounded by a limit cycle for $\mu > \mu_H$, in which μ_H satisfies that

$$K = \frac{2\mu_H^2}{(2\mu_H - 1)\sqrt{\mu_H - \mu_H^2}}.$$

Proof. Substituting $E_4 = (w^*, B^*)$ into (2.4), we obtain the following Jacobian matrix:

$$\begin{pmatrix} r\left(2\mu - 1 - \frac{2\mu^2}{K\sqrt{\mu-\mu^2}}\right) & -\mu \\ \frac{2r\left(K(\mu-1)+\sqrt{\mu-\mu^2}\right)}{K} & 0 \end{pmatrix}. \tag{2.5}$$

The matrix has a trace $T = r\left(2\mu - 1 - \frac{2\mu^2}{K\sqrt{\mu-\mu^2}}\right)$ and a determinant $\Delta = \frac{2r\mu\left(K(\mu-1)+\sqrt{\mu-\mu^2}\right)}{K}$. Given that $\mu < \frac{K^2}{1+K^2}$ (or equivalently, $K < \frac{\mu}{\sqrt{\mu-\mu^2}}$), we have $\Delta > 0$. For the case where $\mu < 0$, it is evident that $T < 0$, establishing stability for E_4 if $\mu < \frac{1}{2}$.

Now, if $\mu > \frac{1}{2}$, an additional condition for stability of E_4 is $K < \frac{2\mu^2}{(2\mu-1)\sqrt{\mu-\mu^2}}$. When $T = 0$, E_4 loses its stability through a supercritical Hopf bifurcation. The Hopf threshold $\mu = \mu_H$ can be expressed by an implicit function, simplified to:

$$K = \frac{2\mu_H^2}{(2\mu_H - 1)\sqrt{\mu_H - \mu_H^2}}. \tag{2.6}$$

The transversality condition for the Hopf bifurcation is satisfied at $\mu = \mu_H$. The coexistence steady state E_4 is stable for $\mu < \mu_H$ and destabilizes for $\mu > \mu_H$, surrounded by a limit cycle.

□

Interestingly, the linear stability results remain unchanged even in the presence of slow-fast timescales. However, the linear stability analysis falls short in capturing the complete dynamics of the slow-fast system (2.3) when $0 < \varepsilon \ll 1$. The system

(2.3) undergoes a catastrophic transition that eludes standard stability analysis. In some cases, the model may tend to overestimate ecological resilience.

To delve into the comprehensive dynamics of the system, we turn to geometric singular perturbation theory and employ blow-up techniques. These approaches, crucial for a nuanced understanding, will be discussed in the upcoming sections.

3. Slow-fast system

In this section, we delve into describing the dynamics of the slow-fast system (2.3). To effectively study the system's dynamics, we analyze the behaviors of the two subsystems corresponding to (2.3) by setting ε to 0. The system's behavior in its singular limit, $\varepsilon = 0$, can be obtained as follows:

$$\begin{cases} \dfrac{\mathrm{d}\omega}{\mathrm{d}t} = f = r\omega\left(1 - \dfrac{\omega}{K}\right) - \dfrac{B\omega^2}{1+\omega^2}, \\ \dfrac{\mathrm{d}B}{\mathrm{d}t} = 0. \end{cases} \tag{3.1}$$

The above system is known as the fast subsystem or layer system corresponding to the slow-fast system (2.3). The rate of change in predator density is 0. In the sense that B can be rewritten as a constant c, determined by the initial condition $B(0) = c$. Therefore, system (3.1) reduces to a degenerate differential equation:

$$\frac{\mathrm{d}\omega}{\mathrm{d}t} = f = r\omega\left(1 - \frac{\omega}{K}\right) - \frac{c\omega^2}{1+\omega^2}, \tag{3.2}$$

with the initial condition $\omega(0) > 0$. The direction of the fast flow depends on the choice of initial conditions $\omega(0)$, $B(0)$, and other parameter values. We use green horizontal lines to indicate the track of system (3.1) in Fig. 1. By expressing system (2.3) in terms of slow time $\tau := \varepsilon t(\varepsilon > 0)$, an equivalent system in terms of slow time is obtained:

$$\begin{cases} \varepsilon\dfrac{\mathrm{d}\omega}{\mathrm{d}\tau} = f = r\omega\left(1 - \dfrac{\omega}{K}\right) - \dfrac{B\omega^2}{1+\omega^2}, \\ \dfrac{\mathrm{d}B}{\mathrm{d}\tau} = g = \left(-\mu B + \dfrac{B\omega^2}{1+\omega^2}\right). \end{cases} \tag{3.3}$$

Substituting $\varepsilon = 0$ into the above system of equations, we obtain the differential algebraic equation (DAE)

$$\begin{cases} f = r\omega\left(1 - \dfrac{\omega}{K}\right) - \dfrac{B\omega^2}{1+\omega^2} = 0, \\ \dfrac{\mathrm{d}B}{\mathrm{d}\tau} = g = \left(-\mu B + \dfrac{B\omega^2}{1+\omega^2}\right), \end{cases} \tag{3.4}$$

which is known as the slow subsystem corresponding to the slow-fast system (3.3). The solution of the above system is constrained to the set

$$\left\{(\omega, B) \in R_+^2 : f\,(\omega, B) = 0\right\}$$

and is known as critical manifold M_0. This set corresponds one-to-one to the equilibrium set of system (3.2). The critical manifold consists of two distinct manifolds

$$M_0^0 = \left\{(\omega,\ B) \in R_+^2 : \omega = 0,\ B \geq 0\right\},$$

$$M_0^1 = \left\{(\omega,\ B) \in R_+^2 : B = q\left(\omega\right) := \frac{r\left(1+\omega^2\right)\left(1-\frac{\omega}{K}\right)}{\omega},\ \omega > 0,\ B > 0\right\},$$

such that $M_0 = M_0^0 \cup M_0^1$, where M_0^0 is the positive v-axis and M_0^1 is a portion of the cubic curve in the first quadrant shown in Fig. 1, which is marked with bluish violet color. The slow flow on the critical manifold is given by

$$\frac{\mathrm{d}\omega}{\mathrm{d}\tau} = \frac{g\left(\omega, B\right)}{q'\left(\omega\right)}.$$

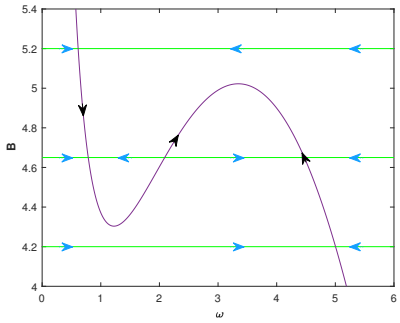

Figure 1. Dynamics of the slow-fast system (2.3) where green line represents slow flow and bluish violet line represents fast flow.

When $\varepsilon > 0$ is sufficiently small, the solution of system (2.3) cannot be approximated by its limiting solution at $\varepsilon = 0$. Thus, $\varepsilon = 0$ is the singular limit of system (2.3). Combined with the solution of the system in its singular limit, the full system solution is obtained. We employ two subsystems based on the region of the phase space. For $r = 2.53, K = 7.348$, and $\mu = 0.62$, the coexistence steady state is unstable for $0 < \varepsilon \leq 1$ and is surrounded by a stable limit cycle. Notably, the size and shape of the stable limit cycle change with the variation of ε, as shown in Fig. 2. The size of the closed curve attractor is significantly different at $\varepsilon = 1$ and $\varepsilon = 0.001$. However, keeping other parameters fixed, as we decrease $\varepsilon \ll 1$, there is a small change in the solution, and the change in the shape of the limit cycle is not clearly distinguishable. This observation is based on numerical simulation, and a detailed analysis is needed to understand the possible shape of the trajectories in the singular limit $\varepsilon \to 0$. For $\varepsilon = 0.001$, the closed curve attractor (depicted in red) consists of two horizontal segments with fast flow and two curved segments with slow flow. This solution can be viewed as a perturbation of the $\varepsilon = 0$ solution achieved by combining the solutions of the layer system (3.1) and the slow subsystem (3.4). The two horizontal segments of the attractor (depicted in red) represent perturbed trajectories associated with the layers, signifying rapid fluctuations in prey species while predator density remains unchanged. The two curvilinear parts closely align with the critical manifold M_0^1. Changes in the shape and size of the

attractor are not solely dependent on the magnitude of ε but also on the parameters related to reaction kinetics and time scale parameters.

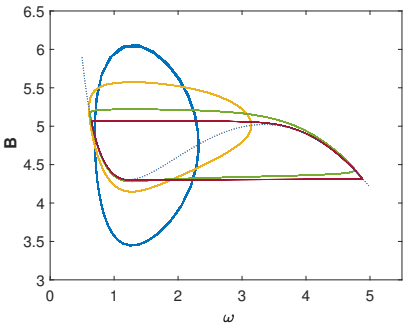

Figure 2. Limit cycles for different values of timescale parameter $\varepsilon = 1$ (blue), $\varepsilon = 0.1$ (orange), $\varepsilon = 0.01$ (green), $\varepsilon = 0.001$(red). Mainfold(dotted line).

When we increase the parameter μ, the image transforms into a canard cycle with a head. Conversely, when we decrease the parameter μ, the image changes to a cycle without a head. It is noteworthy that when $\mu = 0.5999$, the canard cycle without a head transforms into a canard cycle with a head (see Fig. 3).

In the time series image, the transition between the fast, small loop and the slow, large loop is prominently observable. The budworm population experiences rapid reproduction at a specific time, swiftly reaching its peak within a short period, depicted as the sharp vertical rise in (b). Subsequently, the budworm population begins to decline due to bird predation. With an increase in the bird population, this decline accelerates, reaching its minimum. Thereafter, it reverts to a lower count, awaiting the next population surge.

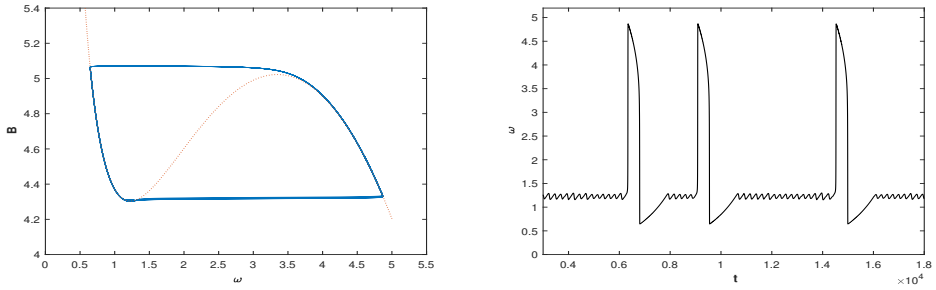

(a) (b)

Figure 3. (a) canard cycle for $\mu = 0.5999$. (b) time series image.

In the next section, we will derive the analytical conditions for the existence of a canard cycle. The analytical results will aid us in identifying the domains in the parametric plane where we can find these different types of closed curve attractors.

4. Analysis of slow-fast system

The critical manifold M_0^1 can be divided into two parts: one part consists of the attractors of the fast subsystem, and the other part is repelling in nature. The attracting and repelling parts of the manifold are separated by a non-degenerate fold point P. The fold point $P(\omega_f, B_f)$ is characterized by the following conditions:

$$\frac{\partial f}{\partial \omega}(\omega_f, B_f) = 0, \quad \frac{\partial f}{\partial B}(\omega_f, B_f) \neq 0, \quad \frac{\partial^2 f}{\partial^2 \omega}(\omega_f, B_f) \neq 0, \quad \text{and} \quad g(\omega_f, B_f) \neq 0.$$

According to the above conditions, we obtain two points: the minimum point $P_1(\omega_1, B_1)$ and the maximum point $P_2(\omega_2, B_2)$ of the critical manifold. The fold point divides the critical manifold into attracting $M_0^{1,a}$ and repelling $M_0^{1,r}$ submanifolds given by

$$M_0^{1,a} = \left\{(\omega, B) \in R_+^2 : B = q(\omega),\ 0 < \omega < \omega_1 \text{ or } \omega_2 < \omega\right\},$$

$$M_0^{1,r} = \left\{(\omega, B) \in R_+^2 : B = q(\omega),\ \omega_1 < \omega < \omega_2\right\}.$$

Define $M_0^{'} = M_0^{1,a} \cup M_0^{1,r}$, and it is straightforward to observe that it is obtained from M_0 by removing the two extreme points P_1 and P_2. All the eigenvalues of $\frac{\partial B}{\partial \omega}(\omega, B)$ that take values on $M_0^{'}$ have nonzero real parts; consequently, $M_0^{'}$ is considered hyperbolic. Clearly, it is also a compact manifold. $M_0^{'}$ plays a crucial role in the research and analysis of M_ε. The relationship between them is explained by the following theorem.

Theorem 4.1. *Let $M_0^{'}$ be a compact normal hyperbolic manifold of system (9). Then for a sufficiently small ε, there exists a manifold*

$$M_\varepsilon = \Big\{ (\omega, B) \in R_+^2 : B = q(\omega,\ \varepsilon) = q_0(\omega) + \varepsilon q_1(\omega) + \varepsilon^2 q_2(\omega), \\ 0 < \omega < \omega_1 \ \text{or}\ \omega_1 < \omega < \omega_2 \ \text{or}\ \omega_2 < \omega \Big\}$$

where

$$q_0(\omega) = \frac{-rmv}{\omega},\ q_1 = \frac{r\,m\,j\,v}{w\,g},$$

$$q_2 = \frac{r\,m\,j\,v\left(\frac{2\,r\,j\,v}{g} - \frac{\mu\,m}{w^2} + \frac{r\,m\left(\frac{2\,\mu}{w} - \frac{2\,\mu\,m}{w^3}\right)v}{w\,g} + \frac{r\,m\,j}{K\,w\,g} - \frac{r\,m\,j\,v}{w^2\,g} - \frac{r\,m\,j\,v\,h}{w\,g^2} + 1\right)}{w\,g^2},$$

$$m = w^2 + 1,\ v = \frac{w}{K} - 1, h = \frac{4\,r}{K} - \frac{2\,r\,v}{w} - \frac{2\,r\,m}{K\,w^2} + \frac{2\,r\,m\,v}{w^3},$$

$$g = 2\,r\,v + \frac{r\,m}{K\,w} - \frac{r\,m\,v}{w^2},\ j = \frac{\mu\,m}{w^2} - 1,$$

such that

(i) M_ε is diffeomorphic to $M_0^{'}$.

(ii) M_ε is locally invariant with respect to the flow of system (2.3).

(iii) For $0 < r < +\infty$, M_ε is C^r-smooth.

Proof. (i) To prove M_ε is diffeomorphic to $M_0^{'}$, it has to prove that there exist two mapping. One mapping is from $M_0^{'}$ to M_ε, and the other mapping which is also the inverse of the previous mapping is from M_ε to $M_0^{'}$.

According to the expression of M_ε and $M_0^{'}$, any point in $M_0^{'}$ can be written $(\omega, q_0(\omega))$ explicitly as

$$q_0(\omega) = \frac{r\left(1+\omega^2\right)\left(1-\frac{\omega}{K}\right)}{\omega}.$$

Any point in M_ε can be written $(\omega, q(\omega,\ \varepsilon))$ as

$$q(\omega,\ \varepsilon) = q_0(\omega) + \varepsilon q_1(\omega) + \varepsilon^2 q_2(\omega).$$

About q_1, it rewrites the format to include q_0,

$$q_1(\omega) = \frac{q_0(\omega)\cdot\left(-1+\mu\frac{1+\omega^2}{\omega^2}\right)}{q_0'(\omega)}. \tag{4.1}$$

Similarly, let q_2 become a form containing q_0 and q_1,

$$q_2(\omega) = \frac{q_1(\omega)\cdot\left(-1+\mu\frac{1+\omega^2}{\omega^2}\right) - q_1(\omega)\cdot q_1'(\omega)}{q_0'(\omega)}. \tag{4.2}$$

Combined with the above expression, then there is

$$\begin{aligned} q(\omega,\ \varepsilon) =& q_0(\omega) + \varepsilon\frac{q_0(\omega)\cdot\left(-1+\mu\frac{1+\omega^2}{\omega^2}\right)}{q_0'(\omega)} \\ &+ \varepsilon^2\frac{\frac{q_0(\omega)\cdot\left(-1+\mu\frac{1+\omega^2}{\omega^2}\right)}{q_0'(\omega)}\left[-1+\mu\frac{1+\omega^2}{\omega^2} - \left(\frac{q_0(\omega)\cdot\left(-1+\mu\frac{1+\omega^2}{\omega^2}\right)}{q_0'(\omega)}\right)'\right]}{q_0'(\omega)}. \end{aligned} \tag{4.3}$$

From the above expression, any point $A(\omega, q_0(\omega))$ in $M_0^{'}$ is mapped to $B(\omega, q(\omega,\ \varepsilon))$ in M_ε. That is to say that the mapping $f : M_0^{'} \to M_\varepsilon$ is founded. Next, let $\varepsilon = 0$ and the following equality holds

$$q_0(\omega) = q(\omega,\ 0). \tag{4.4}$$

Similarly, by the above formula any point $C(\omega, q(\omega,\ \varepsilon))$ in M_ε is mapped to $D(\omega, q_0(\omega))$ in $M_0^{'}$. The map $g : M_\varepsilon \to M_0^{'}$ is founded. And since $M_0^{'}$ and M_ε have the same range of values for ω, f and g are bijective. To sum up, M_ε is diffeomorphic to $M_0^{'}$.

(ii) To prove that $M_\varepsilon = \left\{(\omega, B) \in R_+^2 : F(\omega, q(\omega,\varepsilon)) = B - q(\omega,\varepsilon) = 0\right\}$ is invariant in the sense that

$$F(\omega, q(\omega,\varepsilon))\cdot[0,t] \subset F(\omega, q(\omega,\varepsilon)\cdot[0,t])$$

with respect to the flow of system (9), it means to prove the invariance condition [4]

$$\frac{\mathrm{d}B}{\mathrm{d}t} = \frac{\mathrm{d}q(\omega,\ \varepsilon)}{\mathrm{d}\omega}\frac{\mathrm{d}\omega}{\mathrm{d}t} + O\left(\varepsilon^2\right).$$

Using the explicit expression for $\frac{\mathrm{d}B}{\mathrm{d}t}$ and $\frac{\mathrm{d}\omega}{\mathrm{d}t}$ from (2.3), the equation becomes

$$\left(-\mu B+\frac{B\omega^2}{1+\omega^2}\right)=\varepsilon\frac{\mathrm{d}q\left(\omega,\ \varepsilon\right)}{\mathrm{d}\omega}\left(r\omega\left(1-\frac{\omega}{K}\right)-\frac{B\omega^2}{1+\omega^2}\right)+O\left(\varepsilon^2\right). \tag{4.5}$$

Substituting the expressions for q_0, q_1, and q_2, we verify that the equality holds.

(*iii*) According to the expression of q_0 and the value of the domain of definition, q_0 is continuous. Take into account of the above fact, $q_0^{'}$ is in fractional form and (4.3), we find that M_ε is C^r-smooth.

□

By the above theorem, the expression for M_ε is obtained, which is plotted in the Fig. 4. It reveals the tight connection between M_ε and $M_0^{'}$.

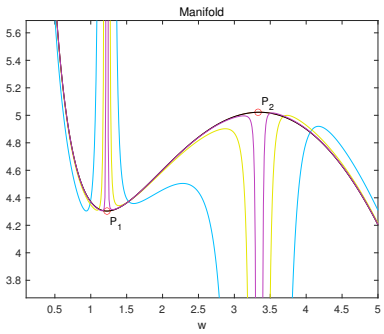

Figure 4. M_ε with $\varepsilon=1$(blue), $\varepsilon=0.1$(yellow), $\varepsilon=0.01$(purple). $M_0^{'}$ (solid black line).

For various ε values, the approximation of invariant manifolds is depicted in Fig. 4. This representation displays two non-removable discontinuities near the non-hyperbolic points P_1 and P_2. The critical manifold $M_0^{'}$ is hyperbolic except at P_1 and P_2, and the same holds for M_ε. Consequently, trajectories originating near the attractor submanifold $M_0^{1,a}$ and the repulsive submanifold $M_0^{1,r}$ cannot pass through the fold points P_1 and P_2. Upon observing Fig. 4, it's evident that for sufficiently small ε, the trajectory closely approaches the attractive manifold $M_0^{1,a}$ and traverses through point P_1.

4.1. Slow-fast normal form

The theory presented in the previous section is insufficient to determine an analytical expression for a perturbed submanifold near M_0^1 that is continuous near a non-hyperbolic point. Therefore, to construct a trajectory passing near point P, it is necessary to remove the singularity associated with this point.

Depending on the parameter μ, the predator nullcline intersects either $M_0^{1,a}$ or $M_0^{1,r}$ or passes through the fold point P_1. Hence, the coexistence equilibrium point E_4 of system (2.3) either lies on $M_0^{1,a}$, or on $M_0^{1,r}$, or coincides with P_1. When E_4 is located on $M_0^{1,a}$, it is globally asymptotically stable, and every trajectory converges to E_4. When E_4 coincides with the fold point P_1, then $f(E_4)=0$, $g(E_4)=0$, $f_\omega(E_4)=0$, $f_B(E_4)\neq 0$, and $f_{\omega\omega}(E_4)\neq 0$. This point is called the canard point. For the system (2.3), the Hopf point coincides with the canard point. The solutions through the vicinity of this point are called canard solutions. For $\mu>\mu_H$, the

coexisting equilibrium point E_4 lies on the repulsive submanifold $M_0^{1,r}$, which is unstable, and we obtain a special periodic solution consisting of two fast flows (almost horizontal) and two slow flows (passing near $M_0^{1,a}$), called relaxation oscillations. We will discuss the existence of such solutions in the following subsections.

To eliminate the singularity at the fold point, we employ a blow-up transformation at the non-hyperbolic fold point, extending the system over a 3-sphere in R^4, denoted by $S_3 = \{x \in R^4 : ||x|| = 1\}$. Through the use of the blow-up technique, we successfully remove the singularity from the system and ascertain the canard solution passing through this point. To facilitate the blow-up technique, we first transform the slow-fast system (2.3) into the desired slow-fast normal form.

The fold point P_1 coincides with the coexisting equilibrium point at $\mu = \mu_*$. Consequently, the following conditions hold:

$$\begin{aligned} &f(\omega_*, B_*, \mu_*) = 0, \quad g(\omega_*, B_*, \mu_*) = 0, \\ &f_\omega(\omega_*, B_*, \mu_*) = 0, \quad f_B(\omega_*, B_*, \mu_*) = 0, \\ &g_\omega(\omega_*, B_*, \mu_*) = 0, \quad g_\mu(\omega_*, B_*, \mu_*) = 0, \\ &f_{\omega\omega}(\omega_*, B_*, \mu_*) = 0. \end{aligned} \tag{4.6}$$

Using the transformation $U = \omega - \omega_*, V = B - B_*, \lambda = \mu - \mu_*$, we translate the fold point to the origin. Together with the conditions (4.6), the system reduces to the slow-fast normal form near $(0, 0)$ as follows:

$$\begin{aligned} \frac{\mathrm{d}U}{\mathrm{d}t} &= -Vh_1(U, V) + U^2h_2(U, V) + \varepsilon h_3(U, V), \\ \frac{\mathrm{d}V}{\mathrm{d}t} &= \varepsilon(Uh_4(U, V) - \lambda h_5(U, V) + Vh_6(U, V)), \end{aligned} \tag{4.7}$$

where

$$\begin{aligned} h_1 &= K(U + \omega_*)^2, \\ h_2 &= r\left(U + \frac{\mu_*}{\sqrt{\mu_* - \mu_*^2}}\right)\left(-U + \frac{-4\mu_*^2 + 3\mu_*}{(2\mu_* - 1)\sqrt{\mu_* - \mu_*^2}}\right), \\ h_3 &= 0, \\ h_4 &= \frac{B_*K(U + 2\omega_*)}{1 + \omega_*^2}, \\ h_5 &= K(V + B_*)(1 + (U + \omega_*)^2), \\ h_6 &= K\frac{U^2 + 2\omega_*U}{1 + \omega_*^2}. \end{aligned} \tag{4.8}$$

4.2. Blow-up

The fold point P_1 and the equilibrium point E_* in system (2.3) coincide with the Hopf bifurcation threshold. Thus, P_1 is a Canard point. We apply a geometric transformation so that the non-hyperbolic equilibrium point is "blown up" into a sphere called the blow-up space [5]. In this case, we consider the blow-up space as a 3-sphere, $S^3 = \left\{(\bar{U}, \bar{V}, \bar{\lambda}, \bar{\varepsilon}) \in R^4 : \bar{U}^2 + \bar{V}^2 + \bar{\lambda}^2 + \bar{\varepsilon}^2 = 1\right\}$. Let $I := [0, \rho]$ where $\rho > 0$ is a small constant, and let $r \in I$. We define a manifold $M := S^3 \times I$ and the blow-up map, $\phi : M \to R^4$ where

$$\phi(\bar{U}, \bar{V}, \bar{\lambda}, \bar{\varepsilon}, \bar{r}) = (\bar{r}\bar{U}, \bar{r}^2\bar{V}, \bar{r}\bar{\lambda}, \bar{r}^2\bar{\varepsilon}) = (U, V, \lambda, \varepsilon). \tag{4.9}$$

Using the above map to study the dynamics of the transformed system on and around the hemisphere S^3_ε, we will introduce the charts with direction blow-up maps [26].

The critical threshold for the transition from the canard cycle without a head to the canard cycle with a head is computed by the following lemma. When exactly this threshold is reached, the canard cycle is called the maximal canard curve.

Lemma 4.1. *[1] Let $(U, V) = (0, 0)$ be the canard point of the slow-fast normal form (18) at $\lambda = 0$ such that $(0, 0)$ is a folded singularity and $G(0, 0, 0) = 0$. Then, for $\varepsilon > 0$ sufficiently small there exists a maximal canard curve $\lambda = \lambda_c(\sqrt{\varepsilon})$, i.e., the parametric curve of maximal canard solution such that the slow flow on the normally hyperbolic invariant submanifolds $M^{1,a}_\varepsilon$ connects with $M^{1,r}_\varepsilon$ in the blow-up space. $\lambda_c(\sqrt{\varepsilon})$ is given by*

$$\lambda_c(\sqrt{\varepsilon}) = -\left(\frac{a_1 + a_5}{2} + \frac{A}{8}\right)\varepsilon + O\left(\varepsilon^{\frac{3}{2}}\right),$$

where $a_1 = \frac{\partial h_3}{\partial x}(0, 0, 0, 0)$, $a_2 = \frac{\partial h_1}{\partial x}(0, 0, 0, 0)$, $a_3 = \frac{\partial h_2}{\partial x}(0, 0, 0, 0)$, $a_4 = \frac{\partial h_4}{\partial x}(0, 0, 0, 0)$, $a_5 = h_6(0, 0, 0, 0)$, and $A = -a_2 + 3a_3 - a_4 - a_5$.

For system 2.3, there is a result given by (4.8). Further, it can be obtained that.

$$\begin{aligned}
&a_1 = 0, \quad a_2 = 2K\omega_*, \quad a_3 = r\frac{-6\mu_H^2 + 4\mu_H}{(2\mu_H - 1)\sqrt{\mu_H - \mu_H^2}},\\
&a_4 = \frac{B_* K}{1 + \omega_*^2}, \quad a_5 = 0,\\
&A = -a_2 + 3a_3 - a_4 - a_5\\
&\quad = -\frac{4\mu_H^2}{(2\mu_H - 1)(1 - \mu_H)} + r\frac{-18\mu_H^2 + 12\mu_H}{(2\mu_H - 1)\sqrt{\mu_H - \mu_H^2}} - r\frac{2}{2\mu_H - 1}.
\end{aligned} \tag{4.10}$$

According to the above lemma and 4.10, the following theorem holds.

Theorem 4.2. *The maximal canard curve, along which the canard cycle with head appears for the system (2.3) is given by*

$$\mu_c = \mu_H + \frac{1}{4}\left(\frac{2\mu_H^2}{(2\mu_H - 1)(1 - \mu_H)} - \frac{2r(-9\mu_H^2 + 6\mu_H)}{(2\mu_H - 1)\sqrt{\mu_H - \mu_H^2}} + \frac{1}{2\mu_H - 1}\right)\varepsilon + O\left(\varepsilon^{\frac{3}{2}}\right).$$

Keeping r, K and $\varepsilon(> 0)$ fixed, then μ_H is going to be fixed. Therefore, μ_c gives the threshold for the existence of canard cycle with a head. A schematic diagram of the threshold curves in $\mu - \varepsilon$ plane is illustrated in Fig. 5 and it divides the $\mu - \varepsilon$ parametric plane into three zones.

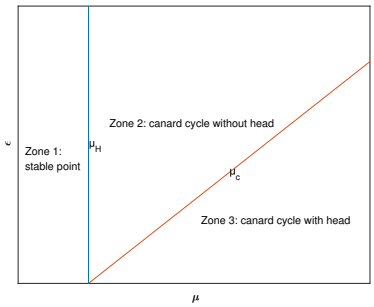

Figure 5. Schematic diagram showing singular Hopf bifurcation curve μ_H (cyan), maximal canard curve μ_c (orange).

In Zone 1, when $\mu < \mu_H$, the coexistence equilibrium point is stable. As we decrease μ from Zone 1 to Zone 2 with a fixed $\varepsilon > 0$, small-amplitude canard cycles appear after crossing the Hopf bifurcation threshold $\mu = \mu_H$.

In Zone 2, where $\mu_H < \mu < \mu_c$, the system undergoes a transition from a canard cycle with a head to a canard cycle without a head. The size of the canard cycle increases as μ is raised, and the cycle transforms into a canard with a head at $\mu = \mu_c$. The canard cycle with a head persists in a narrow Zone 3, where $\mu > \mu_c$.

With further increases in μ, the unstable equilibrium point is surrounded by a stable periodic attractor known as relaxation oscillation. This periodic attractor comprises two concatenated flows: one slow (close to the critical manifold) and the other fast (almost horizontal and away from the critical manifold).

It's noteworthy that for sufficiently small ε, this transition from a small canard cycle to relaxation oscillation through a canard cycle with a head occurs within a narrow interval of the parameter μ, a phenomenon known as canard explosion.

4.3. Canard explosion

In the preceding sub-sections, we observed the periodic dynamics of the slow-fast system near the canard point, where the predator nullcline intersects the non-trivial prey nullcline at the fold point. This intersection occurs at a specific threshold of the parameter μ. At this point, the coexistence equilibrium loses stability through singular Hopf bifurcation, giving rise to a small-amplitude stable limit cycle. As the parameter μ increases, the initially Hopf bifurcating stable cycle grows in size and eventually settles into a relaxation oscillation. The rapid transition in the size of the limit cycle, from small canard cycles to relaxation oscillation, occurs within an exponentially small range of the parameter μ. This phenomenon is commonly referred to as canard explosion.

Now, with $\varepsilon = 0.001$ and keeping other parameters as mentioned above constant, except for μ. A slight variation in μ just above μ_H leads to a rapid change in the size and shape of the periodic attractor (see Fig. 6). A small limit cycle (blue) emerges for $\mu = 0.5995$, referred to as the canard cycle without a head. This cycle undergoes a change in curvature at $\mu = 0.6082$, resulting in the canard cycle with a head (orange). Further increasing μ to 0.7 causes the system to settle into a closed cycle, known as relaxation oscillation. Subsequent increases in μ do not alter the size and shape of the closed attractor, and trajectories converge to the stable

relaxation oscillation cycle for sufficiently small ε.

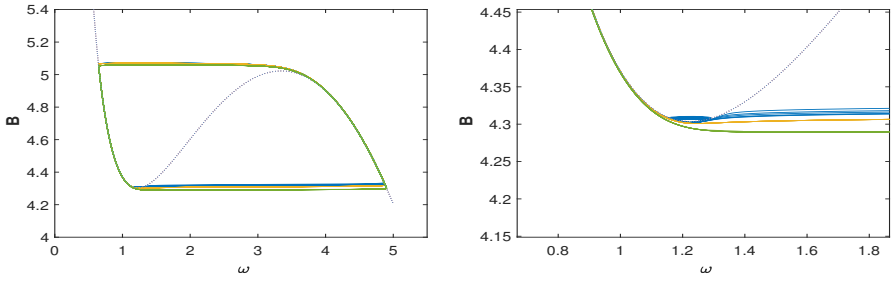

(a) (b)

Figure 6. (a) Canard cycle without head for $\mu = 0.5995$(bule), canard cycle with head for $\mu = 0.6082$(orange), relaxation oscillation for $\mu = 0.7$(green). Mainfold (dotted line). (b) Enlarge figure.

The family of canard cycles is depicted in Fig. 6 for a fixed ε and three values of μ close to the singular Hopf bifurcation threshold μ_H. The coexistence equilibrium is stable for $\mu < \mu_H$, and the trajectory converges to the stable steady state for any initial condition, making it the global attractor.

For μ just above μ_H, a stable limit cycle grows in size, giving rise to a new periodic solution known as the canard cycle without a head (Fig. 6, blue color). This marks the onset of the canard explosion. Upon further increasing μ slightly, another canard cycle, known as canard with head (Fig. 6, orange color), emerges. This cycle is special in the sense that it follows the repelling slow manifold $M_0^{1,r}$ for $O(1)$ time from the vicinity of the fold point before jumping to another attracting manifold. The maximal canard is achieved at $\mu = \mu_c$. After crossing the maximal canard threshold, the system settles down to a large stable periodic solution called a relaxation oscillation, signifying the end of the canard explosion. This orbit is characterized by the fact that the slow flow, upon reaching the vicinity of the fold point, directly jumps to another attracting slow manifold, as studied in the previous section.

As $\varepsilon \to 0$, all trajectories asymptotically converge to a stable limit cycle comprising alternate slow and fast transitions of prey and predator densities. This cycle can be interpreted as follows: when the predator population reaches a high density, there is a rapid decline in the prey population due to excessive consumption by the specialist predator, leading to a significantly low prey level. Consequently, the predator population declines slowly until it reaches a low threshold density, at which point the prey population starts growing again. As a result, the prey regenerates within a very short time while the predator density remains more or less constant. As the prey density approaches its carrying capacity, the predator population grows slowly due to the abundance of resources. Finally, when the predator density reaches its maximum level, the slow-fast cycle completes, and this dynamic continues over time.

5. Discussion

In the present article, we investigated the spruce budworm-bird model with slow-fast timescales, conducting a thorough slow-fast dynamic analysis. During this process,

the blow-up technique [5] was employed to obtain the analytical expression for the singular Hopf bifurcation curve $\mu_H(\sqrt{\varepsilon})$, along which the eigenvalues singularly vary as $\varepsilon \to 0$.

By using Melnikov's distance function in the blow-up space, we explicitly derived a special slow-fast solution known as canards (with or without a head) [27]. In addition, we innovatively determined the analytical expression of the maximum canard curve $\mu_c(\sqrt{\varepsilon})$ of the spruce budworm-bird system. Another type of periodic solution was identified, consisting of two slow and fast flows connected in series, referred to as relaxation oscillations. Finally, we validated our results numerically.

Our findings confirm several intriguing biological phenomena: the populations of the spruce budworm and bird exhibit periodic fluctuations. The spruce budworm undergo rapid reproduction, reaching near environmental capacity within a short timeframe, followed by a gradual decline due to predation by birds over a longer duration. Subsequently, the population stabilizes for a period before the cycle repeats itself over time.

The distinct timescale differences between prey and predator species give rise to interesting features in their respective populations. On the one hand, changes in prey populations occur on faster timescales compared to predator populations, with predator populations remaining almost constant during the rapid growth and decline of prey populations. On the other hand, changes in predator populations occur more slowly relative to prey populations.

Acknowledgements

The authors would like to thank the anonymous referee for several valuable suggestions and comments which helped to improve the paper. This research is supported by National Natural Science Foundation of China [No.12371499].

References

[1] M. Krupa, P. Szmolyan, *Extending geometric singular perturbation theory to nonhyperbolic points - Fold and canard points in two dimensions*, SIAM Journal on Mathematical Analysis, 33 (2) (2001) 286-314.

[2] H.-b. Lu, M.-k. Ni, L.-m. Wu, *Extending slow manifold near generic transcritical canard point*, Acta Mathematicae Applicatae Sinica, English Series, 33 (4) (2017) 989-1000.

[3] M. Krupa, P. Szmolyan, *Relaxation oscillation and canard explosion*, Journal of Differential Equations, 174 (2) (2001) 312-368.

[4] N. Fenichel, *Geometric singular perturbation theory for ordinary differential equations*, Journal of Differential Equations, 31 (1) (1979) 53-98.

[5] F. Dumortier, R. H. Roussarie, *Canard cycles and center manifolds*, Vol. 577, American Mathematical Soc., 1996.

[6] M. Brons, R. Kaasen, *Canards and mixed-mode oscillations in a forest pest model*, Theoretical Population Biology, 77 (4) (2010) 238-242.

[7] M. Brons, M. Desroches, M. Krupa, *Mixed-Mode Oscillations Due to a Singular Hopf Bifurcation in a Forest Pest Model*, Mathematical Population Studies, 22 (2) (2015) 71-79.

[8] J. Moehlis, *Dynamical Systems in Neuroscience: The geometry of excitability and bursting* (2008).

[9] J. Wang, B. Lu, S. Liu, X. Jiang, *Bursting Types and Bifurcation Analysis in the Pre-Botzinger Complex Respiratory Rhythm Neuron*, International Journal of Bifurcation and Chaos, 27 (1) (JAN 2017).

[10] F. Zhan, S. Liu, J. Wang, B. Lu, *Bursting patterns and mixed-mode oscillations in reduced Purkinje model*, International Journal of Modern Physics B, 32 (5) (FEB 20 2018).

[11] F. Diener, M. *Diener, Chasse au canard. i. les canards*, Collect. Math, 32 (1) (1981) 37-74.

[12] F. Zhan, S. Liu, X. Zhang, J. Wang, B. Lu, *Mixed-mode oscillations and bifurcation analysis in a pituitary model*, Nonlinear Dynamics, 94 (2) (2018) 807-826.

[13] B. Lu, S. Liu, X. Jiang, J. Wang, X. Wang, *The mixed-mode oscillations in av-ron-parnas-segel model*, Discrete and Continuous Dynamical Systems-Series S, 10 (3) (2017) 487-504.

[14] M. Wechselberger, *Geometric singular perturbation theory beyond the standard form*, Vol. 6, Springer, 2020.

[15] I. Lizarraga, M. Wechselberger, *Computational Singular Perturbation Method for Nonstandard Slow-Fast Systems*, SIAM Journal On Applied Dynamical Systems, 19 (2) (2020) 994-1028.

[16] S. Rinaldi, S. Muratori, *Slow-fast limit cycles in predator-prey models*, Ecological Modelling, 61 (3-4) (1992) 287-308.

[17] R. Gupta, P. Chandra, *Bifurcation analysis of modified Leslie–Gower predator–prey model with Michaelis–Menten type prey harvesting*, Journal of Mathematical Analysis and Applications, 398 (1) (2013) 278-295.

[18] A. Atabaigi, A. Barati, *Relaxation oscillations and canard explosion in a predator-prey system of Holling and Leslie types*, Nonlinear Analysis-Real World Applications, 36 (2017) 139-153.

[19] D. Ludwig, D. D. Jones, C. S. Holllng, *Qualitative analysis of insect outbreak systems: the spruce budworm and forest*, University of Chicago Press, Chicago, 1978, pp. 547-564.

[20] L. J. Mook, *Birds And The Spruce Budworm*, Memoirs of the Entomological Society of Canada, 95 (S31) (1963) 268-271.

[21] H. S. Crawford, D. T. Jennings, *Predation by birds on spruce budworm choristoneura fumiferana: functional, numerical, and total responses*, Ecology, 70 (1) (1989) 152-163.

[22] P. Arriola, I. Mijares-Bernal, J. Ortiz-Navarro, R. Saenz, *Dynamics of the Spruce Budworm Population under the Action of Predation and Insecticides*, Biometric Department, MTBI Cornell University Technical Report, (01 1999).

[23] X. Xu, J. Wei, *Bifurcation analysis of a spruce budworm model with diffusion and physiological structures*, Journal of Differential Equations, 262 (10) (2017) 5206-5230.

[24] G. Hek, *Geometric singular perturbation theory in biological practice*, Journal of Mathematical Biology, 60 (3) (2010) 347-386.

[25] C. S. Holling, *The functional response of predators to prey density and its role in mimicry and population regulation*, The Memoirs of the Entomological Society of Canada, 97 (S45) (1965) 5-60.

[26] M. Desroches, J. Guckenheimer, B. Krauskopf, C. Kuehn, H. M. Osinga, M. Wechselberger, *Mixed-Mode Oscillations with Multiple Time Scales*, SIAM Review, 54 (2) (2012) 211-288.

[27] P. R. Chowdhury, S. Petrovskii, M. Banerjee, *Oscillations and Pattern Formation in a Slow-Fast Prey-Predator System*, Bulletin of Mathematical Biology, 83 (11) (NOV 2021).